Received: 1 February 2022 | Revised: 3 April 2022 | Accepted: 29 May 2022

DOI: 10.1002/suco.202200107

ARTICLE

fib CEB-FIP WILEY

Mechanical and fractural characteristics of structural lightweight fiber reinforced concrete

Jamshid Esmaeili[1] | **Mahdi Ghaffarinia**[1] | **Mehrab Nodehi**[2] | **Osman Gencel**[3] | **Jinyan Shi**[4] | **Togay Ozbakkaloglu**[2]

[1]Department of Civil Engineering, University of Tabriz, Tabriz, Iran

[2]Ingram School of Engineering, Texas State University, San Marcos, Texas, USA

[3]Civil Engineering Department, Faculty of Engineering, Architecture and Design, Bartin University, Bartin, Turkey

[4]School of Civil Engineering, Central South University, Changsha, China

Correspondence
Togay Ozbakkaloglu, Ingram School of Engineering, Texas State University, San Marcos, TX, USA.
Email: togay.oz@txstate.edu

Osman Gencel, Civil Engineering Department, Faculty of Engineering, Architecture and Design, Bartin University, 74100 Bartin, Turkey.
Email: ogencel@bartin.edu.tr

Abstract

Recent advances in the development of high-performance insulating composite materials have created a new trend in the construction industry for the production of optimized lightweight structural sections. Although such sections are often found to have enhanced strength-to-weight ratio, their lower fracture resistance and toughness are commonly known to prone lightweight concrete sections to brittle failure with a low capacity to withstand crack propagation. To address this, in this study, six mixes containing lightweight expanded clay aggregates with a small quantity of hooked steel fibers ranging from 0 to 1.15 vol% are produced. As a result, it is found that the inclusion of steel fibers at 1.15 vol% can increase fracture energy and characteristic length by about 20 and 11 times, respectively. The result of this study is found to be significant and point to the development of highly ductile, structural-grade lightweight fiber reinforced concrete through the use of hooked steel fibers.

KEYWORDS

characteristic length, expanded clay, fracture energy, lightweight fiber reinforced concrete, steel fiber

1 | INTRODUCTION

The increase in the production of consumer goods, rapid urbanization and development of technology, has increased the dependance in natural resources. At a global scale, construction industry is estimated to use about 20%–50% of natural resources and generate about 50% of total solid waste.[1] To address this, structural optimization and sustainable use of resources have recently received considerable attention. In general, performance-based optimization of structures is a relatively new field that aims to bridge the gap between the structural optimization theory and its practical application to the design and materials' use in structures.[2] For the most part, topology optimization methods have experienced numerous applications and progress in recent decades and have become a key component of aerospace, automobile, and aeronautical industries where the strength to weight ratio and thermal performance of structured composites are of great significance.[2,3] In construction industry, this development took a turn during the 20th century by the discovery of the

Discussion on this paper must be submitted within two months of the print publication. The discussion will then be published in print, along with the authors' closure, if any, approximately nine months after the print publication.

expansion tendency of certain shales and clays when exposed to elevated temperatures.[4,5] This led to their use in numerous industries with the majority of it in construction, as lightweight aggregates in the production of concrete.[4,5] Expanded clay, for instance, is produced through exposure to elevated temperatures of 1100 to 1300°C in kilns.[6] In this process, gaseous fumes are released from the clay particles, causing it to expand about 5 times[6] and produce a highly porous particles with a density of around 350–500 kg/m^3 and a water absorption of ∼14%.[7]

Such use of lightweight aggregates in the production of concrete further allowed the production of low density concrete with a high insulation performance and enhanced earthquake resistance due to the significantly lowered structural deadload.[7] Although there are alternative techniques for reducing the density values of concrete, most commonly, expanded shale, clay, pumice, slate and perlite aggregates are used due to the resulting lower pore network connectivity and better physico-mechanical properties. For instance, lightweight concrete produced with a foaming agent is reported to experience coalescence, ripening and drainage of pores that can result in significant instability of hardened state properties. In turn, lightweight aggregate-based concretes have a higher physico-mechanical properties and are more dependable for structural uses.[7]

Nonetheless, although the use of porous, lightweight aggregates in the production of lightweight concretes has certain benefits, it is commonly reported that a lower ductility is developed. This results in a lower plastic deformation and a brittle fracture when failure occurs. In detail, due to the lower energy absorption of lightweight aggregates, the motion of dislocations and line defects in the atomic lattice become more sudden and does not control crack propagation.[8,9]

In this regard, although fracture properties are generally dependent on the overall stress level and the type of loading (cyclic, static, and even the strain rate), the presence of defects and materials properties is considered to be more fundamental in controlling the crack propagation and fracture mechanism of specimens.[8] In light of this, numerous studies have attempted to increase the fracture toughness, which refers to the resistance toward the propagation of flaws.[8] Notably, the use of nano materials[10] ductile aggregates,[11] and fibers,[12] have been most recently evaluated. Among such possible solutions, the use of fibers in various forms, has been consistently found beneficial in increasing the overall ductility of concrete specimens. For instance, various types of fibers including steel, synthetic, aramid, and glass and carbon fibers, in concrete have been conducted and have produced a higher ductility concretes. Although each type of fibers have its specific effect on the physico-mechanical properties, steel fibers have consistently been found beneficial in the production of concretes with higher plastic deformation due to their high energy absorption capacity and tensile strength.[13] Most commonly, steel fibers are used in form of straight, hook-ended (or hooked) and corrugated.[14] According to the results of References 14,15, the use of hooked steel fibers is the most efficient in enhancing the fiber matrix bond due to its interlocking effect. Yet, the inclusion of steel fibers is often regarded as a costly practice, as it is used mostly in specific structural sections such as ultra-high-performance concrete.[16] In that respect, this study adopted the use of hooked steel fibers in small quantity to enhance the mechanical and fracture properties of lightweight, expanded-clay-based concrete while also being cost effective for practical applications. In this regard, the addition of fibers to the mixtures can significantly affect the cracking and bending properties while since it is used in small quantity, the probability of fiber flocculation or any dispersion issues is minimized.

According to the literature, recent studies in this area have pointed to the effectiveness of steel fiber in mechanical and fracture properties of lightweight concretes. Gao et al.,[17] for instance, studied mechanical properties of steel fiber reinforced concretes and determined the impact of steel fiber on Poisson's ratio, elasticity modulus, and flexural fracture toughness (according to ASTM C 1018[18]). They showed that by the inclusion of steel fiber, compressive strength was lightly, and the ratio of tensile-to-compressive strength, was notably improved. Reference 17, however, did not provide an in-depth evaluation of fracture properties of steel fiber reinforced lightweight concrete. In turn, Christidis et al.[19] studied the mechanical properties of lightweight concrete utilizing pumice as the aggregate and hooked steel as fiber reinforcement. They found that flexural and compressive strengths enhanced remarkably while a multi-phase model was suggested for the prediction of crack propagation. Hassanpour et al.[20] focused on the properties of lightweight fiber reinforced concrete with low volume fractions of steel fibers (≤1%) and reported that compressive, tensile and flexural strengths at 28 days increased by 32%, 77%, and 69%, respectively, only by adding 1 vol% steel fibers to the mixture. As before, this study also did not evaluate the fracture properties of the produced specimens. Xie et al.[21] reviewed fibers effect on recycled aggregate concrete characteristics and indicated that the workability decreased by adding fibers, however, through crack-bridging action durability and mechanical properties improved. Additionally, they reported steel fibers, comparing with other fibers, performed better in enhancing the mechanical properties. Zhao et al.[22] developed an experimental work applying sintered fine and coarse expanded shale aggregates and study impacts of compressive strength and steel fiber volume in expanded-shale-based lightweight concrete. In their analysis, it was reported that after peak load, fibers increased the toughness significantly. Celik and Bingol[23] studied the fracture properties of polypropylene reinforced self-compacting concrete and

TABLE 1 Physico-chemical properties of OPC

Properties	Percent
SiO_2	21.34
CaO	64.13
Fe_2O_3	3.73
MgO	2.11
Na_2O	0.21
K_2O	0.55
Tetracalcium aluminoferrite	11.38
Dicalcium silicate	22.21
Sulfite	2.22
Chloride ion	0.01
Free lime	1.13
Silica modulus	2.37
Tricalcium silicate	51.73
Alumina modulus	1.41
Tricalcium aluminate	7.62
Insoluble residue	0.67
Lime to silica ratio	3.10
Lime saturation factor	91.43
Loss on ignition	0.85
Alite and belite	73.90

TABLE 2 Mechanical properties of cement

Mechanical properties	Value
Fineness (Blaine)	3850
Le Chatelier Expansion	1
Residue on 90 μ Sieve	0.9
Autoclave expansion	0.15
Initial setting time	120
Final setting time	190
Density	3.15
Two days Comp. strength (MPa)	22
1 week Comp. strength (MPa)	39
28 days Comp. strength (MPa)	52

TABLE 3 Chemical properties of silica fume

Chemical composition	Percent
SiO_2	95.6
CaO	0.49
Al_2O_3	1.32
Fe_2O_3	0.87
MgO	0.97
Na_2O	0.30
P_2O_5	0.17

reported significant fracture energy improvement but did not use steel fiber nor did this study used lightweight aggregates. Based on this literature review, although there have been studies that have utilized steel fibers in lightweight concrete, the fracture properties of steel fiber reinforced lightweight concrete containing a low quantity of fibers (~1.15 vol%) has not been evaluated. This evaluation can show the high effectiveness of including a very small quantity of steel fiber to practical mixes to significantly alter the fracture properties of the built sections. In that respect, this study initially evaluates the mechanical properties of the produced specimens and then the fracture characteristics are evaluated based on previous studies and the tests conducted in this research.

2 | MATERIALS AND TEST METHODS

2.1 | Materials

2.1.1 | Cementitious materials

Ordinary Portland Cement (OPC) type I-42.5 based on ASTM C150 was acquired from Soufian Company in East Azerbaijan, Iran. Chemical analysis of OPC is demonstrated in Table 1 and mechanical characteristics are illustrated in Table 2, as well. The silica fume as an active pozzolan in the form of powder with 95.6% silicon dioxide (SiO_2) content and a specific gravity of 2.22 was used. Chemical composition of silica fume is shown in Table 3.

2.1.2 | Aggregate

In this study, expanded clay was used as coarse aggregate with a commercial name of LECA™. The coarse aggregates' maximum size was 12.5 mm. Figure 1a and Table 4 demonstrate shape and physical properties of expanded clay, respectively. For fine aggregates natural river sand from a local quarry with physical properties listed in Table 4 was utilized. Figure 2 further represents the grading curves for both coarse and fine aggregates conducted based on ASTM C330[24] and ASTM C33.[25]

2.1.3 | Steel fiber

Steel fibers were provided by Zanjan Wire Industries Company, in the form of two ends hooked for reinforcement of

the concrete (Figure 1b). The length and length-to-diameter ratio of the fiber are 30 mm and 37.5, respectively. Features of used fibers were summarized in Table 5.

2.1.4 | Admixture

A high performance polycarboxylate-based superplasticizer with commercial name of Structuro 335 was used to enhance workability. Table 6 demonstrates the properties of the aforementioned superplasticizer.

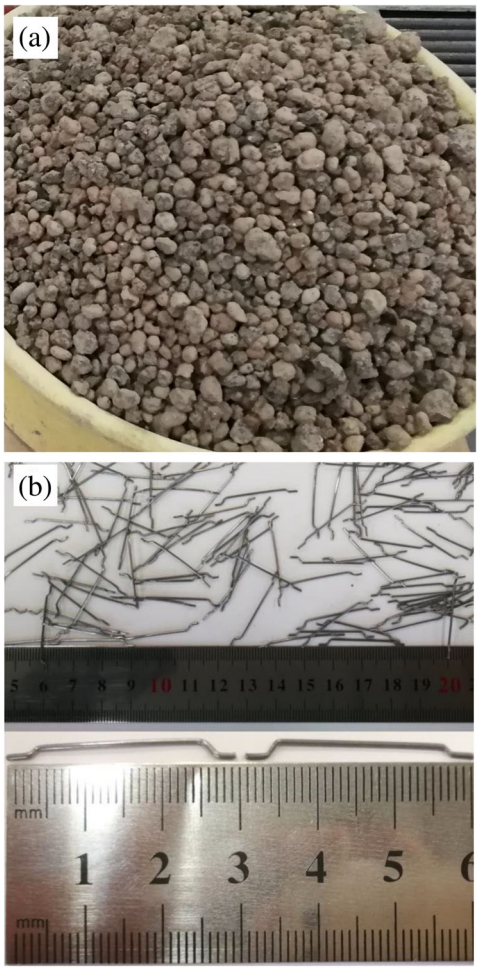

FIGURE 1 Expanded clay as coarse aggregate (a) and hooked steel fiber (b)

2.2 | Mixture proportions and concrete production

To investigate the properties of the specimens, one control mixture (SF0) and five Lightweight fiber reinforced concretes (SF10 to SF90) were developed in current research. The steel fiber contents utilized in mixtures are 10, 20, 30, 60, and 90 kg/m^3 by weight, equivalent to 0.13, 0.26, 0.38, 0.77, and 1.15 percent by volume. The labeling of mixture proportions is as follows: The term SF refers to steel fiber and the numbers after it, indicate the fiber content in weight per 1 cubic meter of concrete. To attain equal yield of fresh concrete in mixes with varying amounts of steel fiber, the amount of sand is decreased volumetrically to compensate the growth of steel fiber. Mixing design of this experiment is further shown in Table 7.

To mix the materials, a pan type mixer with a maximum capacity of 56 l was used. For each steel fiber content the following specimens are prepared and tested accordingly: three beams of 150 × 150 × 550 mm were used in bending tests (based on ASTM C78[26]), five cubic specimens with size of 100 × 100 mm and 3 cylinders with size of 100 × 200 mm (based on ASTM C109[27] and ASTM C39[28]) were used for compressive strength evaluation. Further, 3 cylinders of 150 × 300 mm size were employed to evaluate concretes' elastic modulus (based on ASTM C469[29]) and finally, 6 cylinders with a size of 100 × 200 was prepared for splitting tensile tests (based on ASTM C496[30]).

To ensure a homogenous mix, before starting mixing process, silica fume and superplasticizer was introduced to water and mixed to become homogeneous; then, expanded clay and river sand were mixed for 120 s while half of water was introduced constantly during mixing. In the next step cement was added to the mixture. Mixing processes was continued for 2 min and the unused water was finally added to the mixed materials while the

TABLE 4 Coarse and fine aggregate's physical properties

Expanded clay		River sand	
Relative density (OD)	1.05	Relative density (OD)	2.58
Relative density (SSD)	1.21	Relative density (SSD)	2.61
Absorption (%)	14.95	Absorption (%)	1.5
Bulk density of aggregate (kg/m^3)	713	Fineness modulus	2.83
Voids (%)	72.6		
Bulk density in SSD condition (kg/m^3)	820		

mixing process continued for 1 more minute. Finally, to avoid fiber balling phenomena, fibers were added gradually by sieving process to avoid size variation of fibers (similar to References 31,32), while mixing was under progress. Addition of fibers helped the fresh concrete to gain better particle distribution. The total mixing period of materials was around 6 min. In the casting process, the molds were filled with concrete to about 90% of the height and compacted using an external vibration table. Then they were refilled and leveled off while compaction was under progress. Curing of the fresh specimens was conducted as discussed by ASTM C192.[33] As for the curing regime, after casting, wet burlap was used to cover the concrete and a plastic sheet was placed over burlap to keep it wet. Specimens were cured in 22°C and demolded after 24 h. Then they were immersed in water, saturated with calcium hydroxide until the test date. Figure 3 shows further information on the testing setup used in this study.

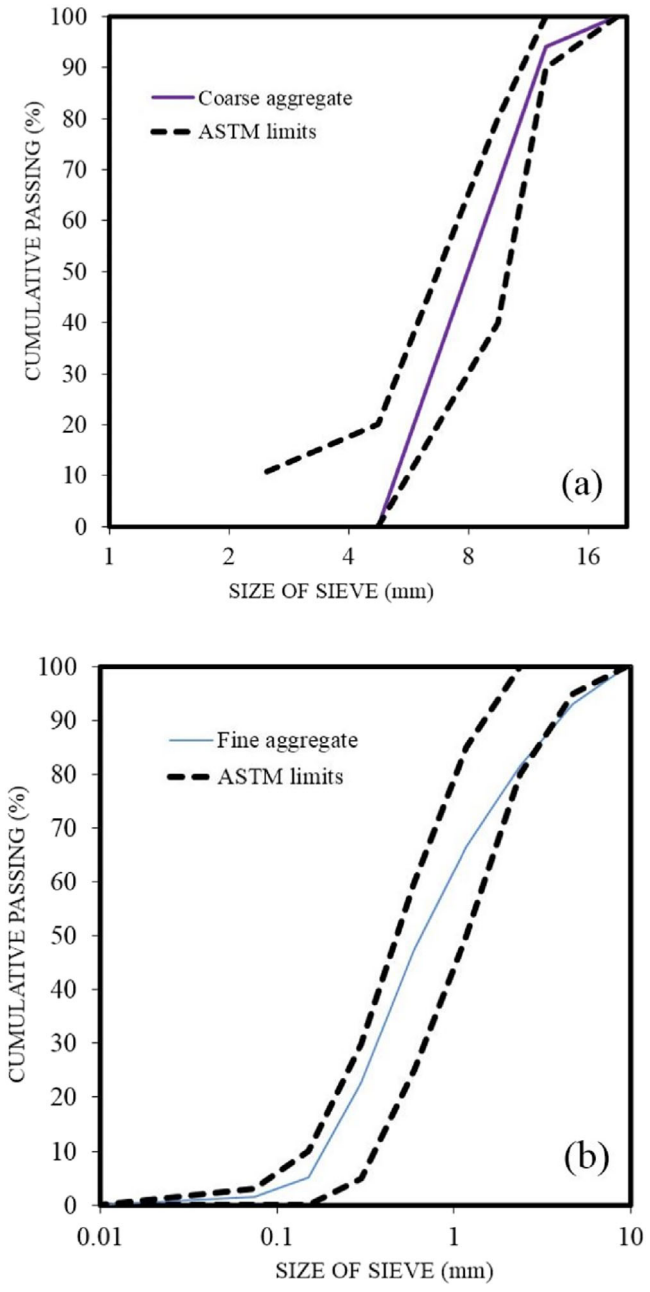

FIGURE 2 Coarse (a) and fine (b) aggregate grading curves and limits of ASTM C33

2.3 | Test methods

Different standards are introduced with various indexes for expressing post-cracking nature of steel fiber reinforced concrete. In this study, Rilem TC 162[34] was taken as the base test method of this research proposed more readily measurable concepts of equivalent and residual flexural tensile strengths ($f_{eq}.f_{R.i}$) to assess modeling of steel fiber reinforced concrete behavior after cracking. In this method, two deflection limits were introduced (δ_2, δ_3) representative of serviceability and ultimate limit states, respectively. Energy absorption capacity ($D_{BZ.2}, D_{BZ.3}$) are achieved from area below load–deflection plot until deflection limits of (δ_2, δ_3). Evaluated energy absorption ability is quantified from summation of the following two components: The first one is energy absorption ability of plain concrete (D^b_{BZ}). Second component is energy absorption capacity due to fibers' presence ($D^f_{BZ.2}, D^f_{BZ.3}$). Figure 4 schematically illustrates the

TABLE 6 Properties of superplasticizer

Appearance	Light yellow colored liquid
PH	6.5
Volumetric mass	1.06 kg/l @ 20°C
Chloride content	<0.1%
Alkali content	Less than 1.5 g Na_2O equivalent/l of admixture

TABLE 5 Characteristics of steel fiber

Length (mm)	Diameter (mm)	Min tensile strength (MPa)	Modulus of elasticity (MPa)	Ultimate strain (DI)	Number of fiber/1 kg
30	0.8	990	200,000	<4%	8000–8100

energy absorption capacity concept in load–deflection curve.

The experimental program was planned to observe impact of the amount of steel fiber on fracture energy, energy absorption, compressive and tensile behavior of lightweight fiber reinforced concrete. In this investigation, Rilem TC 162-TDF,[34] ASTM C 469,[30] and ASTM C496[35] were used as the basis to conduct bending test, elasticity modulus and splitting tensile test, respectively.

Flexural strength test was carried out using center-point loading tests on beams with 500 mm span. So as to exclude extraneous deflection due to supports settlement, crushing of concrete in loading point and torsion of the beam, a yoke (rectangular jig) was settled on the concrete to quantity net deflection of neutral axis.[36,37] A closed-loop universal testing machine (UTM) having maximum 1000 kN loading was utilized to conduct the experiments. Loading process was deformation-controlled type to simulate the quasi-static loading conditions with 0.2 mm/min CMOD opening ratio. Midspan deflection was obtained via placing 2 LVDTs at both sides from beam. By taking average of recorded data of the two LVDTs net deflection. Along with LVDTs for deflection recordings, to gain the CMOD data at notch tip simultaneously, a measuring device (clip gauge) was employed. The test setup and details of the beam (from initial stages to start of the test) are exhibited in Figures 5 and 6.

3 | RESULTS AND DISCUSSION

3.1 | Compressive strength

The result of 28-day compressive strength test results are presented in Figure 7 and Table 8. Based on this figure and the table, the highest and lowest compressive strength values of cubic samples 50.2 MPa for SF60 and 48.6 MPa for SF0 mixes, respectively. As can be seen, this shows about 3% increase when 0 and 60 kg/m^3 (0.66 vol%) fiber content is used. The increase in compressive strength values

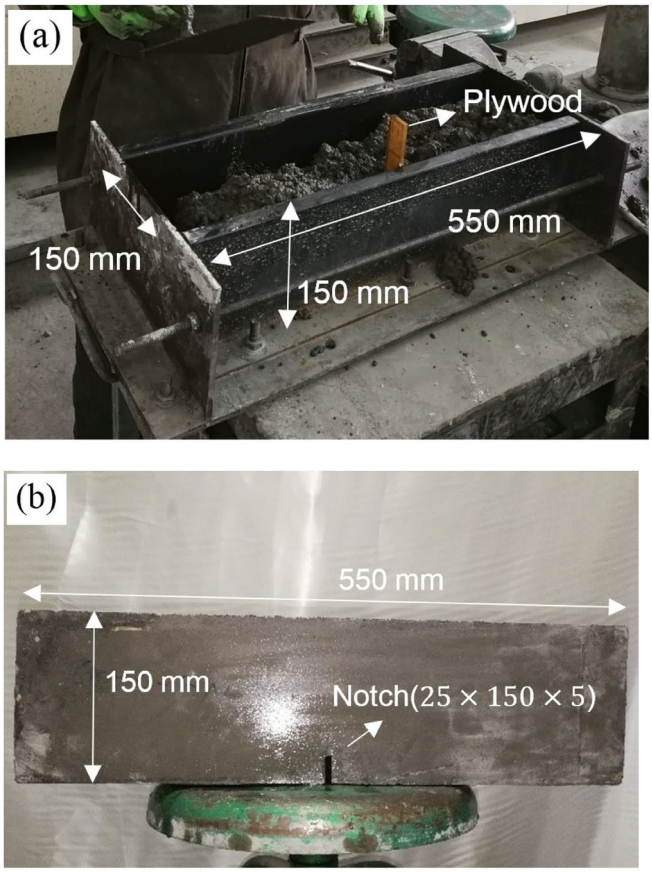

FIGURE 3 (a) Casting beam concrete and (b) beam specimen after removing mold

TABLE 7 Mixture proportion for 1 m^3 of concrete

Material		Mixtures					
		SF0	SF10	SF20	SF30	SF60	SF90
Expanded clay	(kg)	359.3	359.3	359.3	359.3	359.3	359.3
Natural sand	(kg)	946.9	943.6	940.3	937	927	917
Cement	(kg)	418.5	418.5	418.5	418.5	418.5	418.5
Silica fume	(%)	7	7	7	7	7	7
	(kg)	31.5	31.5	31.5	31.5	31.5	31.5
Superplasticizer	(%)	0.61	0.61	0.61	0.61	0.61	0.61
	(kg)	2.75	2.75	2.75	2.75	2.75	2.75
Steel fiber	V_f(%)	0	0.13	0.26	0.38	0.77	1.15
	(kg)	0	10	20	30	60	90
Water	w/c	0.36	0.36	0.36	0.36	0.36	0.36
	(lit)	163.35	163.35	163.35	163.35	163.35	163.35

of mixes containing steel fibers is aligned with References 38–40. For instance, Yazici et al.[41] reported 4%–19% increase in compressive strength of mixes containing 0.5%–1.5% steel fiber. In both studies, a linear ascending pattern is found that the increase in steel fiber content increases the compressive strength values which is discussed in detail by Reference 22. Similar pattern is found for cylinder samples with the highest and lowest compressive strength values achieved for SF0 and SF60, respectively. Further from Figure 7, it can be seen that at 1.15 vol% steel fiber content (SF90) the compressive strength results have experienced slightly lowered value in both cubic samples and cylinders. According to literature,[41,42] this can be due to the flocculation and lack of good dispersion of steel fibers that takes place, especially at higher fiber quantities. Further from Figure 7, it can be seen that the mean difference between cube and cylinder samples is ~21%. This result is aligned with the mean value of the 28-day result of Reference 43 with mean value of ~31 versus 25 for cube and cylinder samples that show a 23% variation. Other studies such as References 44,45 have also documented the same results.

3.2 | Modulus of elasticity

The result of elastic modulus at 28th day of curing is presented in Figure 8a while Figure 9 shows the test set up conducted according to ASTM C469.[29] Table 9 also provides further details on the values achieved. Considering the effect of lightweight coarse aggregate used in this study, the elasticity modulus values are generally lower than normal concrete mixes reported in literature.[46–48] Based on the results, the highest and lowest modulus of elasticity values is for SF90 and SF0 by 22.7 and 21.7 GPa, respectively. As can be seen, a linear relationship can be found between the steel volume included in

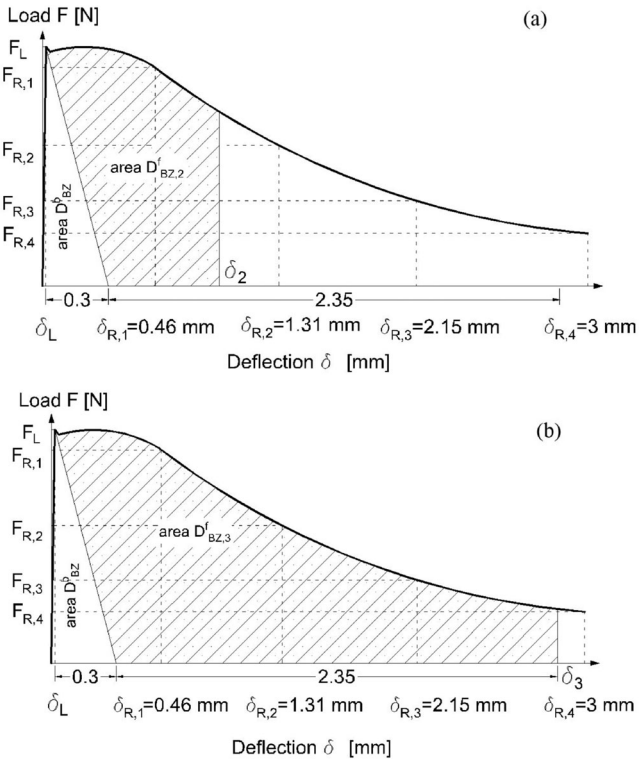

FIGURE 4 Energy absorption capacity concept by Reference 34 (a) $D^f_{BZ.2}$, (b) $D^f_{BZ.3}$.

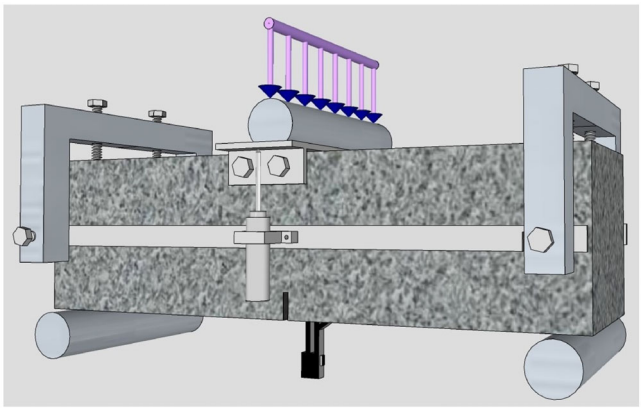

FIGURE 6 Three-point bending test setup

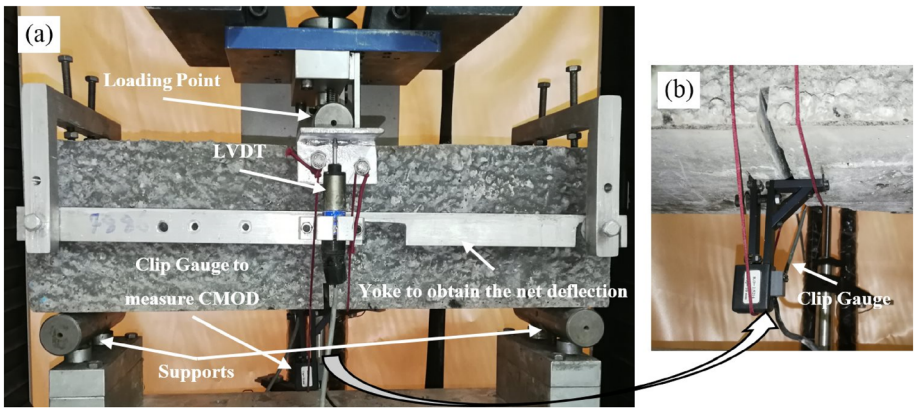

FIGURE 5 (a) Bending test setup and details, (b) clip gauge

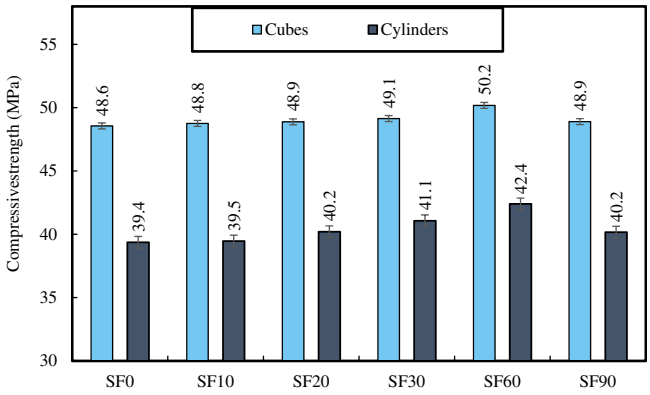

FIGURE 7 Compressive strength of cubic and cylindrical specimens

the mixes and the result of elastic modulus test. Based on Figure 8a,b, a ~5% increase in modulus of elasticity is achieved after the inclusion of 1.15 vol% steel fiber. The increase in the elastic modulus values is due to the very high modulus of steel fibers. Figure 8c also presents the modulus of elasticity calculated based on ACI 318–19[49] and the equation below:

$$E_c = w_c^{1.5}\, 0.043 \sqrt{f_c'}\ (\text{in MPa}) \tag{1}$$

where E_c is the elastic modulus, w_c is density and considered as 1800 kg/m^3, and f_c' represents compressive strength.

TABLE 8 Cubic and cylindrical compressive strength

Fiber content	Cubic compressive strength (MPa)	Mean value and standard deviation (MPa)	Cylinder compressive strength (MPa)	Mean value and standard deviation (MPa)
SF0	48.6	48.6, 1.0	40.4	39.4, 1.6
	50.0		37.1	
	47.1		40.6	
	47.8			
	49.3			
SF10	46.2	48.8, 2.0	39.8	39.5, 0.5
	47.6		38.7	
	48.3		39.9	
	49.5			
	52.2			
SF20	47.5	48.9, 1.0	38.5	40.2, 1.3
	48.1		40.5	
	49.7		41.6	
	49.0			
	50.1			
SF30	50.1	49.1, 0.5	40.7	41.1, 0.9
	48.6		42.3	
	49.2		40.2	
	48.8			
	49.0			
SF60	50.1	50.2, 0.6	41.1	42.4, 0.9
	49.6		43.2	
	50.3		42.9	
	51.3			
	49.6			
SF90	48.0	49.3, 1.1	40.5	40.2, 1.0
	49.9		38.8	
	48.2		41.2	
	49.5			

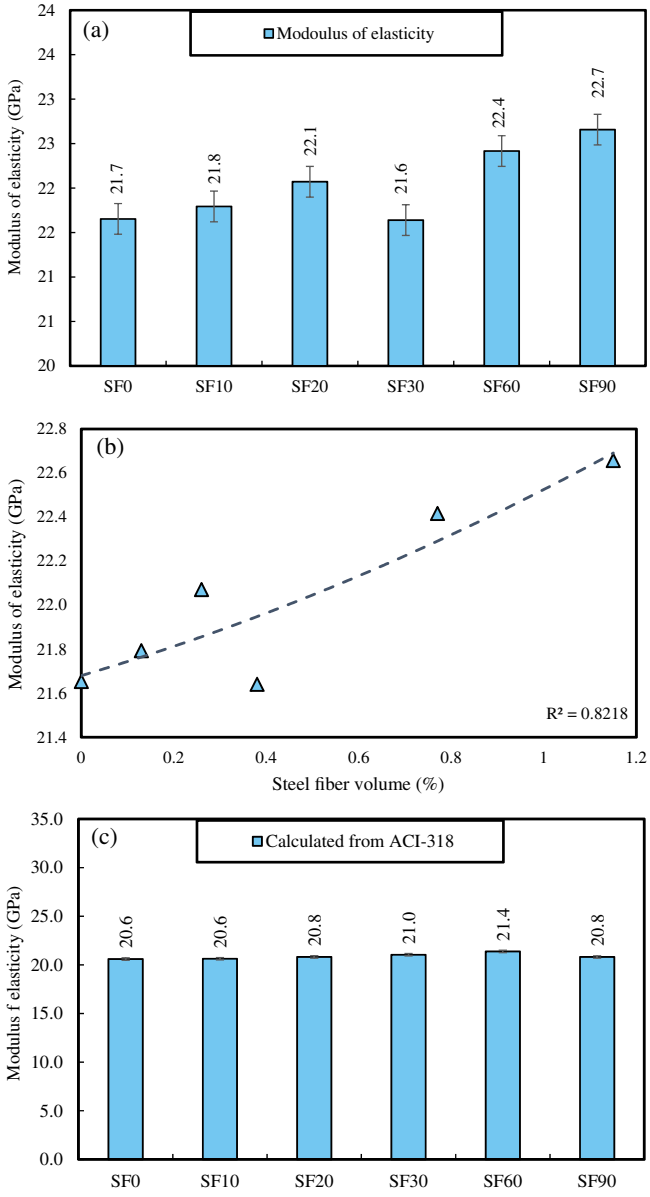

FIGURE 8 (a) Modulus of elasticity of mixes and (b) the relationship between volume of steel fiber and modulus of elasticity

Based on Figure 8c, the range of results is found to be relatively similar with only difference in SF30 which can be due to statistical error.

3.3 | Splitting tensile strength

Splitting tensile experiments were conducted using six cylinders of Ø100 × 200 mm. It was quantified by the relation:

$$T = \frac{2P}{\pi l d} \tag{2}$$

where P, l, and d are maximum load, height and width of specimen, respectively. Figure 10 shows the setup and details of test and the results are all given in Table 10.

FIGURE 9 Modulus of elasticity setup

Based on Figure 11a, an increase in fiber rate is found to considerably affect the splitting tensile strength, as expected and a growth of 1.5%, 3%, 22.7%, 37.9%, and 39.4% was observed in specimens of SF10, SF20, SF30, SF60, and SF90 respectively, compared to the specimen without fiber. Earlier studies, such as Iqbal et al.[50] showed that an increase of 37% in strength of lightweight self-compacting concrete provided by fiber amount ranging from 0% to 1.25% which confirms to results obtained in this study. Similarly, Balendran et al.[39] presented a growth of 33.3% for prismatic splitting strength of lightweight fiber reinforced concrete with fiber amount of 72 kg/m^3 which is comparable to results of this study. Kayali et al.[51] reported an increase of about 79% for indirect tensile strength of lightweight fiber reinforced concrete with a steel fiber content of 88 kg/m^3, which is almost two times of the current study. Similar results from other studies, (e.g., References 52,53) have also been documented for lightweight fiber reinforced concrete that show the high effectiveness of increasing the ductility of this class of concrete. Further from Figure 11b, the relationship between splitting tensile and the steel fiber content is found to be exponential. This shows higher effectiveness of steel fiber in bendability of specimens produced with higher fiber content. Similarly, Figure 11c shows that the splitting tensile to compressive strength ratio continues to be increased as the steel fiber content increases. This figure presents the higher impact of steel fiber on splitting tensile strength, compared to compressive strength values.

TABLE 9 Amounts of the modulus of elasticity

Fiber content	Elasticity modulus (N/mm^2)	Mean value (N/mm^2)	Standard deviation (N/mm^2)	Coefficient of variation (%)
SF0	21,377	21,653	520	2.4
	21,200			
	22,381			
SF10	22,253	21,793	592	2.7
	20,957			
	22,170			
SF20	21,181	22,071	631	2.9
	22,568			
	22,465			
SF30	20,532	21,640	816	3.8
	22,475			
	21,914			
SF60	21,963	22,416	372	1.7
	22,412			
	22,874			
SF90	22,689	22,657	134	0.6
	22,803			
	22,480			

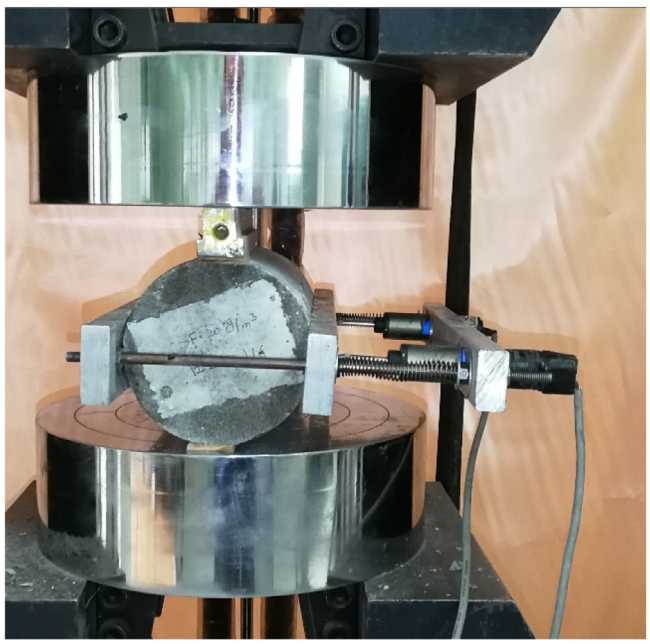

FIGURE 10 Splitting test setup

3.4 | Flexural strength

Figure 12 represents a comparison of typical test results of load–deflection for specimens with different steel fiber contents acquired during bending experimental tests. A general behavior of steel fiber reinforced lightweight concrete is described by an ascending linear portion up to initial cracking point and persisted with a nonlinear behavior until the peak load and eventually carried on with a descending portion throughout complete failure. After first cracking, because of bridging action of the fibers, constant crack spread occurs in midspan section. As the maximum load is approached, the load reduction began to occur and the amount of the loss is inversely related to fiber volume content. Moreover, results shown in Table 11 demonstrate that by a rise in steel fiber content, the maximum load increases correspondingly. Considering the mean peak load values of SF60 and SF90, it can be seen that a growth of 6.6% and 12.4% is occurred, respectively, compared to fiber-free specimens. Table 11 also illustrates the residual load values at $\delta = 3$. It is apparent that the higher presence of the fibers resulted in higher residual loads. As observed in Table 11, the residual loads are increased from 10.4% of the peak load in SF0 to about 43.2% of the peak load in SF90 specimens (Figure 13). Furthermore, in specimens SF10, SF20, and SF30 an abrupt decrease is apparent in load bearing ability instantly after peak load, but, this sudden drop is not present in SF60 and SF 90 and a smooth softening of the curve can be observed, which indicates a complete stable behavior during the experimental test. Figure 13 demonstrates a specimen with steel fiber content of 60 kg/m^3 at its failure position. Figure 14a shows the flexural strength of various

TABLE 10 Splitting tensile strength

Fiber content	Splitting tensile strength (MPa)	Mean value (MPa)	Standard deviation (MPa)	Coefficient of variation (%)
SF0	3.75	3.30	0.3	8.6
	3.40			
	2.95			
	3.25			
	3.00			
	3.55			
SF10	3.45	3.35	0.1	4.3
	3.50			
	3.35			
	3.15			
	3.15			
	3.45			
SF20	3.25	3.40	0.2	5.9
	3.60			
	3.10			
	3.40			
	3.35			
	3.70			
SF30	4.10	4.05	0.2	3.8
	3.95			
	4.05			
	4.30			
	4.10			
	3.80			
SF60	4.35	4.55	0.2	5.1
	4.70			
	4.55			
	4.90			
	4.65			
	4.20			
SF90	4.60	4.60	0.1	2.6
	4.55			
	4.60			
	4.60			
	4.45			
	4.85			

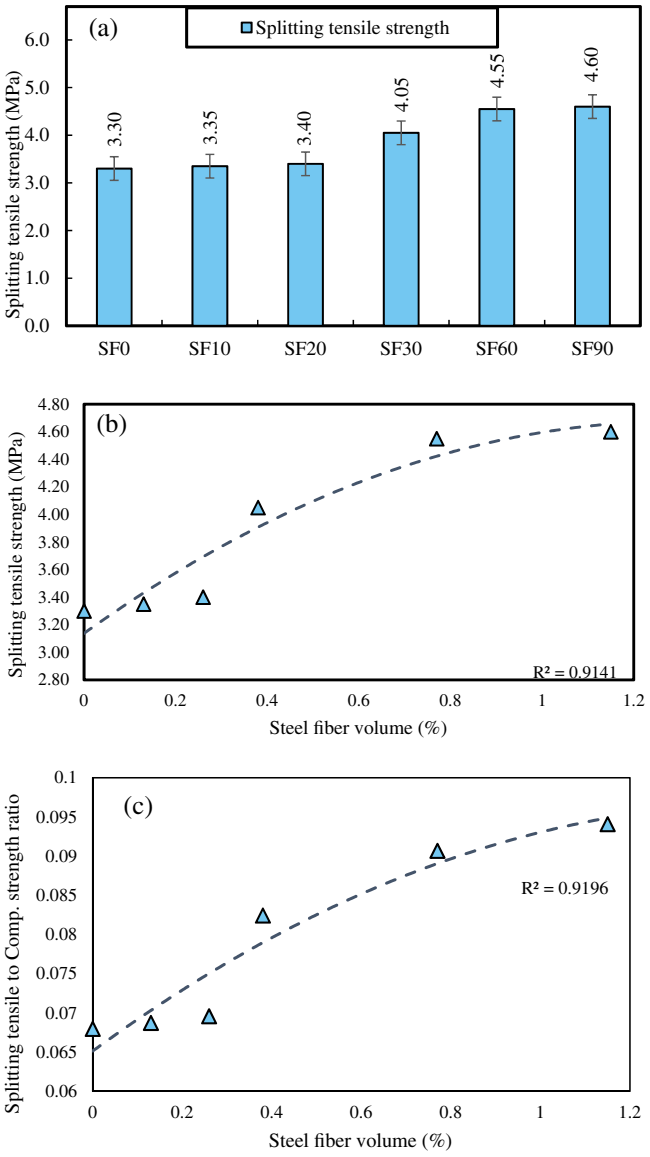

FIGURE 11 Splitting tensile strength of mixes

mixes and (b) ratio of flexural strength versus steel fiber content. Based on Figure 14b a linear relationship between steel fiber content and flexural strength is seen. In this regard, as the content of steel fiber increases, the flexural strength also goes higher. Nonetheless, based on the results outlined and as can be seen in Figure 14c, the inclusion of steel fiber has had a considerably higher effect on increasing the flexural than compressive strengths. This is seen to be exponentially increasing as the steel fiber content increases in Figure 14c.

Figure 15 shows the post-test cracking of samples. Based on Figure 14a,b, for specimens without fibers (SF0) a complete brittle failure with separation of the beam into two parts were occurred at a deflection of about 0.03–0.04 mm. On the other hand, specimens with fibers showed more ductile behavior and the separation of the beam did not occur in these specimens for deflections greater than 3 mm (Figure 14c,d). Additionally, the deflection matching to peak force grows with increment in fiber content, as concluded by Gao et al.,[17] as well.

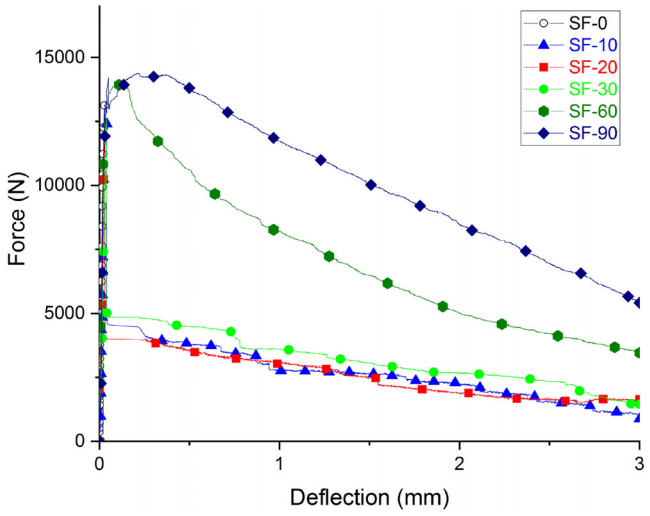

FIGURE 12 Experimental curves of load–deflection

Further, the peak load deflection is mostly in range of between 0.03 and 0.5 mm for all specimens.

3.5 | Fracture properties

The load corresponding to the end of proportionality (F_L) or simply flexural strength is extracted, as the maximum value of the force in the deflection or crack mouth opening displacement (CMOD) range of zero to 0.05 mm. Strength matching to this load ($f_{fct.L}$) is calculated by Equation (3):

$$f_{fct.L} = \frac{3F_L S}{2B(D-a_0)^2} \tag{3}$$

where S is span length, B is beam width and $(D-a_0)$ is ligament height. Deflection limits of δ_2 and δ_3 are obtained as $\delta_2 = \delta_L + 0.65$ and $\delta_3 = \delta_L + 2.65$, where δ_L is deflection matching for F_L. Equivalent flexural tensile strengths are computed from the following expressions:

$$f_{eq.2} = \frac{3S}{2B(D-a_0)^2}\frac{D^f_{BZ.2}}{0.5}\,(\text{MPa}) \tag{4}$$

$$f_{eq.3} = \frac{3S}{2B(D-a_0)^2}\frac{D^f_{BZ.3}}{2.5}\,(\text{MPa}) \tag{5}$$

where $f_{eq.2}$ and $f_{eq.3}$ correspond to deflection limits of δ_2 and δ_3, respectively. In these expressions, first component of total absorbed energy which belongs to plain concrete (D^b_{BZ}) is not present and thus take no role for equivalent strength.

Residual flexural strengths ($f_{R.i}$) represents remaining strength of material after peak load in specified deflections ($\delta_{R.i}$). These deflections of the midspan were equal to 0.46, 1.31, 2.15, and 3 mm, respectively for $\delta_{R.1}$ to $\delta_{R.4}$. For calculation of residual flexural strength, following expression was utilized:

$$f_{R.i} = \frac{3}{2}\frac{F_{R.i}S}{2B(D-a_0)^2}\,(\text{MPa}) \tag{6}$$

All the relations mentioned above are extracted by assumption of a linear stress distribution within undeformed condition of the ligament. Table 12 summarizes all the discussed expressions.

Based on Table 12, the average value of the flexural strength ($f_{fct.L}$) for the specimens of SF90 was increased by 7.7% compared to plain lightweight specimens. Balendran et al.[39] carried out similar bending three-point test on notched beams of 100 × 100 × 500 mm and for flexural strength they obtained an increase of 8.9% with steel fiber content of 72 kg/m^3. In the values of equivalent flexural tensile strength, a remarkable increase was obtained by increment in fiber amounts. In this regard, it can be seen that the mean value of flexural tensile strength for SF90 is improved up to 4.4 and 3.3 times when compared to that of SF10 for deflection limits of δ_2 and δ_3 respectively. Furthermore, it can be noticed that the strength of boundary of proportionality ($f_{fct.L}$) and equivalent flexural strength (f_{eq}) are inversely related to the steel fiber content. As the $f_{fct.L}$ and (f_{eq}) are directly proportional to (F_L), and (D^f_{BZ}) respectively. Further, it was concluded that the ratio of change in absorption of specimens having higher fiber contents surpasses the rate of change in F_L.

3.6 | Fracture energy and characteristic length

Fracture energy (G_F), as stated by cohesive crack model, is the required energy to develop unit area of crack.[54,55] As basic factor in fracture characteristics of quasi brittle materials, such as concrete, G_F was determined with different proposed experimental tests including direct tensile, wedge splitting, and bending tests. Uniaxial tensile test is a mean to gain G_F. However, accomplishing a stable tensile test is rather difficult and precise servo-controlled systems, as well as stiff loading machines are often necessary. Bending tests are most common tests that are used to measure the G_F in concrete. On this basis, in this research, notched beams subjected to bending test suggested by Rilem TC 162[34] were applied. Two approaches were applied to

TABLE 11 Three point bending tests: peak loads and residual loads at $\delta = 3$ mm and load decay percentage

Fiber content	Peak load (kN)	Mean value (kN)	Standard deviation (kN)	Residual load at $\delta = 3$ mm (kN)	Residual load to peak load percentage (%)
SF0	11.8	12.1	0.2	—	—
	12.3			—	—
	12.4			—	—
SF10	11.9	12.2	0.8	1.2	10.4
	13.3			0.9	6.7
	11.5			1.5	12.8
SF20	12.7	12.3	0.3	1.6	12.9
	12.2			2.1	17.1
	11.9			2.4	20.3
SF30	12.6	12.6	0.4	1.4	11.3
	12.0			4.1	34.5
	13.0			2.6	19.9
SF60	12.7	12.9	0.3	4.1	32.5
	12.7			4.4	34.5
	13.3			5.4	41.0
SF90	12.7	13.6	0.7	4.8	38.2
	14.0			3.5	24.8
	14.2			6.1	43.2

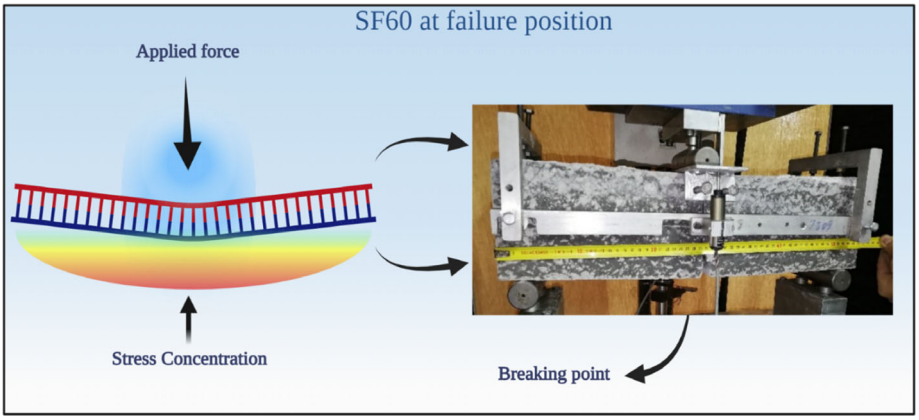

FIGURE 13 Specimen SF60 at failure position

calculate the G_F of the specimens under bending test. In the first procedure the concept of work-of-fracture technique modified for concrete by Hillerborg[56] is applied which is then adopted by Rilem TC 50.[56] According to the method, fracture energy was obtained via dividing total absorbed energy to cross-section area of ligament in undeformed condition of three-point notched beam bending test. Therefore, G_F is calculated via Equation (7):

$$GF = \frac{W_F}{B(D - a_0)} \tag{7}$$

where W_F is amount of total absorbed energy in the notched beam and B is beam width and $(D - a_0)$ is ligament height. A comprehensive examination of this method was explained by Bazant and Planas.[57] More studies established by Guinea, Planas and Elice[54,58,59] explored the procedure for possible error causes during the test and calculations. In beam bending test, the self-weight of the sample participates in the loading system and causes an increase in the moment value in beam. This is commonly termed as weight compensation, which should be considered in fracture energy evaluation. The

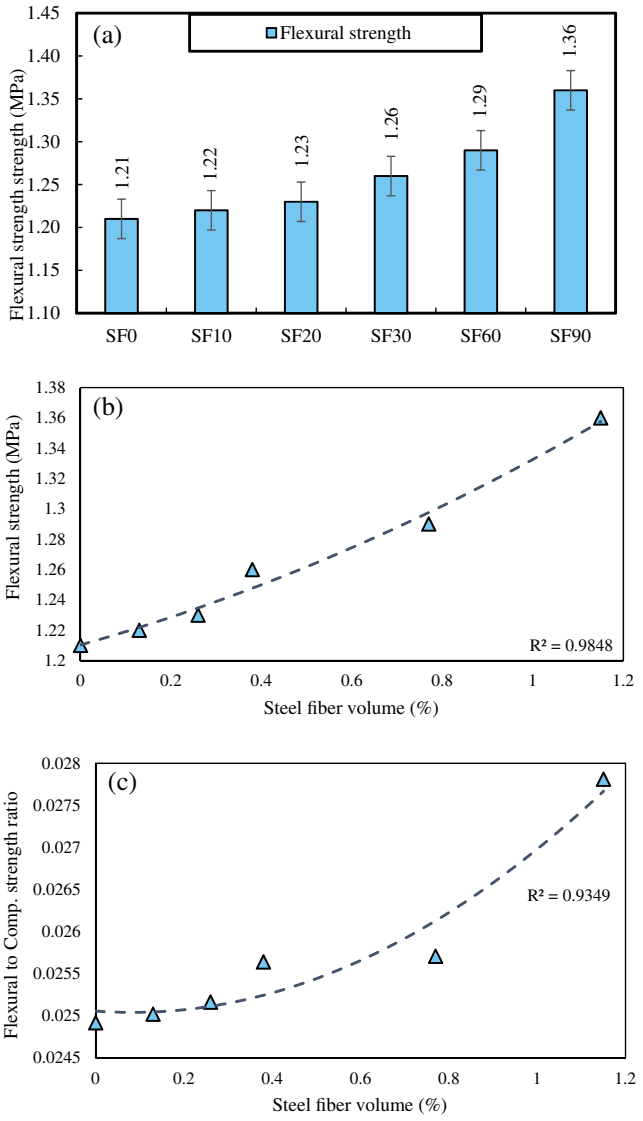

FIGURE 14 (a) Flexural strength of various mixes and (b) ratio of flexural strength versus steel fiber content

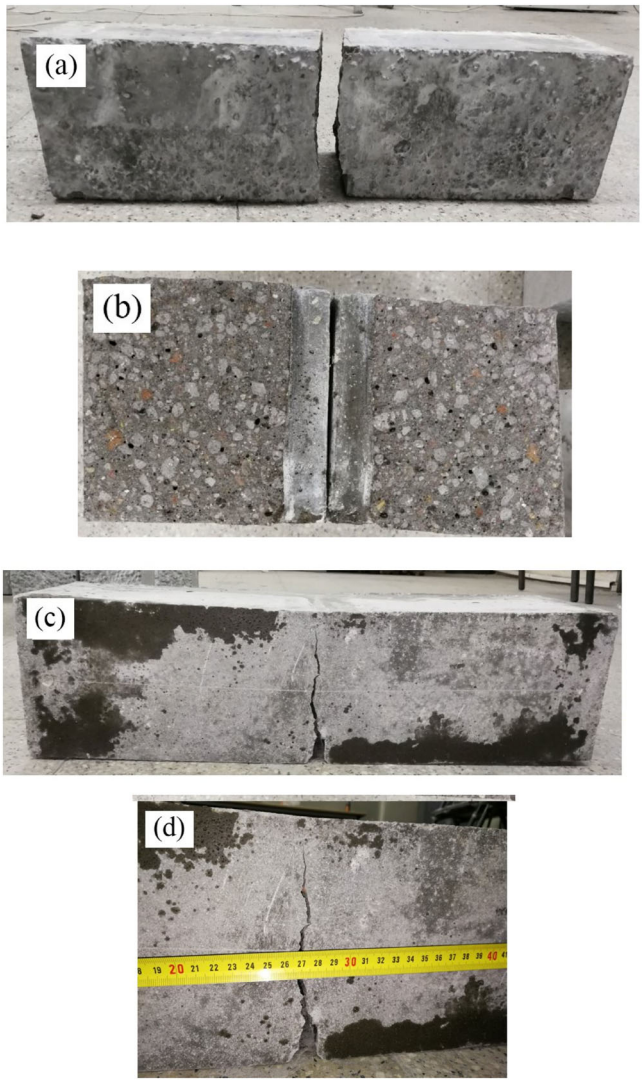

FIGURE 15 Post-test deformed and cracked condition of notched beam specimens (a)-(b) without fibers, (c)-(d) with fibers (SF20)

use of weight compensation was not suggested by Rilem TC 50-FMC,[56] and an analytical correction is used instead. Figure 15 shows a load–displacement curve extracted from a bending test. Generally, in order to take care of measuring instruments, test is terminated at about point B, formerly the beam is completely halved. The axes represented in dashed lines exhibited the best experiment in which specimen was fully separated in 2 splits. To obtain real effort to fracture for notched beam (W_F), amount of W_m (area AMB in Figure 16) is extracted and a correction analysis which can be found in References 57,59 for compensating early test stop. The total work to fracture the specimen is:

$$W_F = W_m + 2\Delta u_0 \Delta P_0 = W_m + 2\frac{BS}{4\Delta u_0}\mu \tag{8}$$

where μ is a constant, related to the softening function. To determine this constant, alternatively by assuming the expression $\frac{BS}{4}\mu = \omega$, as explained in Reference 54, ω can be extracted by least square fitting of:

$$P - P_B = \omega\left[\frac{1}{(u-u_A)^2} - \frac{1}{(u_B-u_A)^2}\right] \tag{9}$$

Thus, given that the $(P-P_B)$ is plotted virsus $(u-u_A)^{-2} - (u_B-u_A)^{-2}$, then ω can be determined by least square matching of straight line through origin.

In second technique, area under stress-displacement plot adopted by Bencardino et al.[60] was utilized to determine the fracture energy. By considering linear spreading of stress in ligament height, the following relation can be obtained for tensile stress:

TABLE 12 Three-point bending tests: fracture properties

Fiber content	F_L (kN)	$f_{fct,L}$ (N/mm^2)	$f_{eq,2}$ (N/mm^2)	$f_{eq,3}$ (N/mm^2)	$f_{R,1}$ (N/mm^2)	$f_{R,2}$ (N/mm^2)	$f_{R,3}$ (N/mm^2)	$f_{R,4}$ (N/mm^2)
SF0	11.8	3.8	—	—	—	—	—	—
	12.3	3.9	—	—	—	—	—	—
	12.2	4.0	—	—	—	—	—	—
Mean	12.1	3.9	—	—	—	—	—	—
SD	0.2	0.1	—	—	—	—	—	—
SF10	11.9	3.8	0.9	0.7	1.1	0.8	0.5	0.2
	12.3	3.9	1.0	0.8	1.2	0.9	0.6	0.1
	11.5	3.7	0.8	0.8	1.0	1.0	0.8	0.2
Mean	11.9	3.8	0.9	0.8	1.1	0.9	0.6	0.2
SD	0.3	0.1	0.1	0.0	0.1	0.1	0.1	0.0
SF20	12.7	4.0	0.9	0.8	1.3	0.9	0.6	0.3
	12.2	3.9	1.3	1.1	1.6	1.3	0.9	0.3
	11.9	3.8	1.1	0.9	1.4	1.2	0.9	0.4
Mean	12.3	3.9	1.1	0.9	1.4	1.1	0.8	0.3
SD	0.3	0.1	0.2	0.1	0.1	0.2	0.1	0.1
SF30	12.6	4.0	2.0	1.8	2.7	1.8	1.1	0.2
	12.0	3.9	2.4	1.9	2.5	1.6	1.0	0.7
	13.0	4.2	2.2	1.7	2.0	1.1	0.8	0.4
Mean	12.5	4.0	2.2	1.8	2.4	1.5	1.0	0.4
SD	0.4	0.1	0.2	0.1	0.3	0.3	0.1	0.2
SF60	12.7	4.1	3.0	2.3	3.2	2.3	1.8	0.7
	12.7	3.7	3.4	2.4	3.4	2.4	1.7	0.7
	13.0	4.5	3.3	2.6	3.7	2.6	1.8	0.9
Mean	12.8	4.1	3.2	2.4	3.4	2.4	1.8	0.7
SD	0.1	0.3	0.2	0.1	0.2	0.1	0.0	0.1
SF90	13.7	3.9	3.5	2.5	3.5	2.4	1.9	0.8
	14	4.3	3.9	2.6	3.5	2.3	1.5	0.6
	14.2	4.5	4.4	2.5	3.6	2.5	1.8	1.0
Mean	14.0	4.2	3.9	2.5	3.5	2.4	1.7	0.8
SD	0.2	0.2	0.4	0.0	0.0	0.1	0.2	0.2

$$\sigma = \frac{3FS}{2B(D-a_0)^2} \tag{10}$$

where F denotes the amount of external load applied to specimen through the experiment. Obtaining the tensile stress, G_F can be calculated using the expression:

$$G_F = \int_{\delta=0}^{\delta=\delta_{lim}} \sigma d\delta \tag{11}$$

where δ_{lim} is a prescribed deflection limit. Ozalp et al.[61] recommended a limiting deflection of 10 mm as cut-off point for steel fiber reinforced concrete. Barros et al.[62] suggested this deflection as 3 mm which is important from the design perspective. In this research as used in References 60,62 3 mm is chosen to be used for fracture energy calculations in second approach.

To evaluate the degree of the ductility or brittleness of concrete, the GF value solely does not suffice. Alternatively, a material parameter suggested by Hillerborg

et al.[63] entitled as the characteristic length (l_{ch}) can be utilized as defined by the following equation:

$$l_{ch} = \frac{EG_F}{f_t^2} \tag{12}$$

Equation (11) shows that l_{ch} was straightly proportional to fracture energy which indicates that a higher fracture energy leads to more ductile concrete, and at the same time having an inverse relation with squared tensile strength, which signifies that high tensile strength results in more brittle concrete for the constant E and G_F. Consequently, a balance between G_F and f_t is needed to obtain ductile concrete.

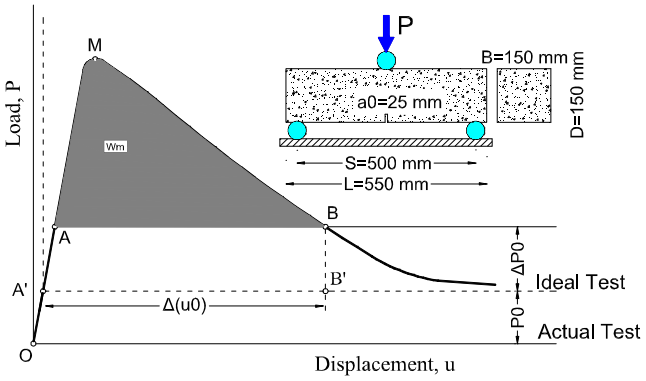

FIGURE 16 A general load–displacement curve for weight compensation concept

The results obtained for all specimens using both approaches are summarized in Table 13. From this table, it is apparent that the values obtained for G_F from second approach are 4–6 times higher than the values derived from first approach. The reason for this difference lies in the nature of Equations (6) and (10) in which the former is originally developed to be used for plain concrete, while the latter is more suitable for steel fiber reinforced concrete. As could be expected, by increasing the amount of fiber's content in lightweight fiber reinforced concrete, the fracture energy also rises in value. For specimens of SF90, GF increased averagely 5.5 and 3.7 times compared to that of SF10 based on the two approaches, respectively. According to Figure 17, the change in fracture energy with respect to fiber content is increased linearly, as conformed to the results of Barros and Cruz.[64]

Furthermore, it can be seen that an increasing trend is clear for characteristic length with increasing the content of fibers. As the steel fiber content increases, tensile strength increases, as mentioned in Table 10. However, the rate of growth for both ratios of fracture energy and elasticity modulus exceeds the rate of growth for squared tensile strength, and thus, the final result has an

TABLE 13 Fracture energy and characteristic length

Fiber content	G_F (1st approach) [N/mm]	l_{ch} (1st approach) [mm]	Mean value [mm]	G_F (2nd approach) [N/mm]	l_{ch} (2nd approach) [mm]	Mean value [mm]
SF0	0.15	298.3	225.3	0.06	119.3	132.6
	0.10	198.8		0.07	139.2	
	0.09	179.0		0.07	139.2	
SF10	0.39	757.3	822.1	2.3	4466.4	4790.0
	0.47	912.7		2.6	5048.9	
	0.41	796.2		2.5	4854.8	
SF20	0.52	992.8	992.8	3.7	7064.2	6809.7
	0.54	1031.0		3.6	6873.3	
	0.50	954.6		3.4	6491.5	
SF30	0.77	1015.9	1117.0	5.5	7256.2	7212.2
	0.84	1108.2		5.8	7652.0	
	0.93	1227.0		5.1	6728.5	
SF60	1.48	1602.5	1689.1	6.9	7471.1	7759.8
	1.61	1743.3		7.1	7687.7	
	1.59	1721.6		7.5	8120.8	
SF90	2.38	2548.4	2480.6	9.1	9743.8	9993.6
	2.42	2591.2		9.5	10,172.1	
	2.15	2302.1		9.4	10,065.0	

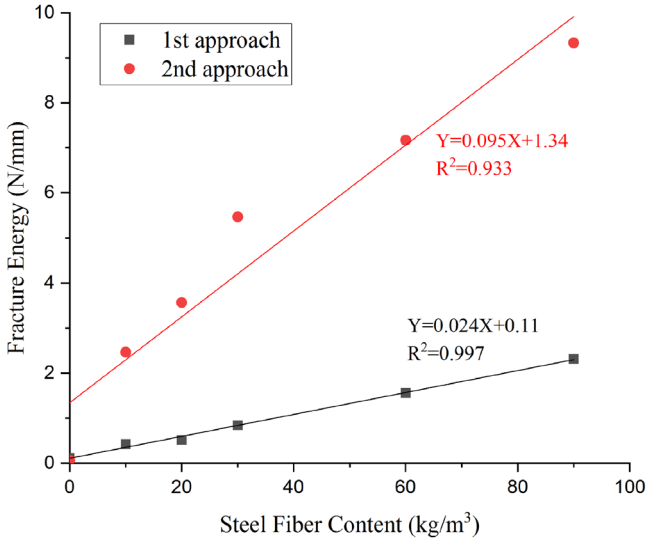

FIGURE 17 Changes of fracture energy with steel fiber content

increasing trend for characteristic length which means a higher ductility. As confirmed to Guneyisi et al.,[65] the characteristic length considerably affected by usage of steel fibers and significantly increased. From Table 13, the increment of characteristic length in the first approach for steel fiber contents of 10, 20, 30, 60, and 90 kg/m^3 is 3.6, 4.4, 5.0, 7.5, and 11.0 times of the specimen with no fibers, while for second approach the increase of the characteristic length for the aforementioned steel fiber contents is 36.1, 51.4 54.4, 58.5, and 75.4 times of the 0% steel fiber volume fraction specimen, respectively.

4 | CONCLUSIONS

In this study, an experiment was conducted to examine the influence of hooked steel fiber on mechanical and fractural characteristics of lightweight concrete. Based on the results, following key findings can be summarized:

- The inclusion of steel fibers in this study is found to have a marginal influence on the compressive strength values. In this regard, the strength values increased by 3% when 0.66 vol% steel fiber (SF60) was used, compared to fiber-free specimens. However, in SF90 specimens (1.15 vol% steel fiber), due to higher amount of entrapped air, compressive strength values were reduced by 1.8%, when compared to SF60 specimen. Additionally, it is found that cubic samples have about 20% higher compressive strength values, compared to their cylinder companions.
- Similar to the compressive strength values, by including steel fibers, the modulus of elasticity increased by a slight amount of 4.6% in SF90 specimens compared to specimens without fibers, which can be accounted for the steel fibers' high modulus of elasticity. In terms of splitting tensile strength, however, the inclusion of steel fibers caused a noticeable increase in the strength values of specimens by 1.5%, 3%, 22.7%, 37.9%, and 39.4% in SF10, SF20, SF30, SF60, and SF90, respectively, compared to fiber-free specimens.
- For mixes with the content of 0.13 and 0.26 vol% steel fiber, the three-point bending test peak load increase were minor of 0.8% and 1.7%, respectively, compared to SF0. On the other hand, for mixes with fiber content of 0.38, 0.77, and 1.15 vol% the increased bending peak load was about 4.1%, 6.6% and 12.4%, with respect to fiber-free samples. The residual load at deflection of 3 mm for specimens of SF10, SF20, SF30, SF60, and SF90 was 10.0%, 16.8%, 21.9%, 36.0%, and 35.4%, respectively, of their corresponding peak load.
- The equivalent flexural tensile strengths were affected notably by increasing the fibers content. For SF20 to SF90 mixes, the average value of $f_{eq.2}$ was increased by 1.2, 2.4, 3.6, and 4.3 times, respectively, with respect to SF10. For these specimens the average value of $f_{eq.3}$ was experienced an increase of 1.1, 2.3, 3.0, 3.1 times of SF10 specimen.
- The fracture energy (G_F) values are increased by adding the amount of steel fibers, as expected. Two approaches, one for normal concrete and the other for fiber reinforced concrete were considered for calculating the fracture energy: In first approach, the fracture energy for specimens of SF10 to SF90 was averagely increased by 3.7, 4.6, 7.5, 13.8, and 20.4 times, respectively, compared to SF0. Alternatively, as the second approach is essentially for fiber reinforced concrete, the results are compared with SF10 specimens. In specimens of SF20 to SF90 the fracture energy average value was about 1.4, 2.2, 2.9, and 3.8 times compared to that of SF10 samples.
- To characterize the ductility of the lightweight fiber reinforced concrete, characteristic length was evaluated, based on two different approaches. Quantitatively, for mixes with steel fiber content of 10 to 90 kg/m^3 (0.13–1.15 vol%), the characteristic length was respectively increased by 3.6, 4.4, 5.0, 7.5, and 11.0 times when compared to fiber-free specimens, based on the first approach. For the second approach, for mixes with steel fiber content of 20–90 kg/m^3 (0.26–

1.15 vol%) this parameter increased by 1.4, 1.5, 1.6, 2.1 times of SF10 samples.

ACKNOWLEDGMENT

The authors appreciate all the universities that supported this study.

DATA AVAILABILITY STATEMENT

Data sharing not applicable to this article as no datasets were generated or analysed during the current study.

ORCID

Mehrab Nodehi https://orcid.org/0000-0001-5896-6375
Jinyan Shi https://orcid.org/0000-0002-6641-2097

REFERENCES

1. Vasilca IS, Nen M, Chivu O, Radu V, Simion CP, Marinescu N. The management of environmental resources in the construction sector: an empirical model. Energies. 2021;14(9):1–19. https://doi.org/10.3390/en14092489
2. Quan Liang Q. Performance-based optimization of structures: theory and applications. Boca Raton, FL: CRC Press; 2004.
3. Chateauneuf A. Principles of reliability-based design optimization. Boca Raton, FL: CRC Press; 2008. p. 3–30.
4. Chandra S, Leif B. Lightweight aggregate concrete. 1st ed. Norwich, NY: William Andrew; 2002.
5. Owens P, Newman J. Structural lightweight aggregate concrete. Glasgow, UK: Blackie Academic & Professional; 1993.
6. Rashad AM. Lightweight expanded clay aggregate as a building material – an overview. Construct Build Mater. 2018;170:757–75. https://doi.org/10.1016/j.conbuildmat.2018.03.009
7. Nodehi M. A comparative review on foam-based versus lightweight aggregate-based alkali-activated materials and geopolymer. Innov Infrastruct Solut. 2021;6(4):231. https://doi.org/10.1007/s41062-021-00595-w
8. Mouritz AP. Fracture processes of aerospace materials. Introduction aerospace materials. New York, NY: Elsevier; 2012. p. 428–53.
9. van der Giessen E, Needleman A. Dislocation dynamics for plasticity boundary value problems. Encyclopedia of materials: metals and alloys. New York, NY: Elsevier; 2022. p. 541–51.
10. Afzali-Naniz O, Mazloom M. Fracture behavior of self-compacting semi-lightweight concrete containing nano-silica. Adv Struct Eng. 2019;22(10):2264–77. https://doi.org/10.1177/1369433219837426
11. Nikbin IM, Farshamizadeh M, Jafarzadeh GA, Shamsi S. Fracture parameters assessment of lightweight concrete containing waste polyethylene terephthalate by means of SEM and BEM methods. Theor Appl Fract Mech. 2020;107:102518. https://doi.org/10.1016/j.tafmec.2020.102518
12. Choi J, Zi G, Hino S, Yamaguchi K, Kim S. Influence of fiber reinforcement on strength and toughness of all-lightweight concrete. Construct Build Mater. 2014;69:381–9. https://doi.org/10.1016/j.conbuildmat.2014.07.074
13. Liew KM, Akbar A. The recent progress of recycled steel fiber reinforced concrete. Construct Build Mater. 2020;232:117232. https://doi.org/10.1016/j.conbuildmat.2019.117232
14. Wu Z, Shi C, He W, Wu L. Effects of steel fiber content and shape on mechanical properties of ultra high performance concrete. Construct Build Mater. 2016;103:8–14. https://doi.org/10.1016/j.conbuildmat.2015.11.028
15. Wu Z, Shi C, Khayat KH. Investigation of mechanical properties and shrinkage of ultra-high performance concrete: influence of steel fiber content and shape. Compos B Eng. 2019;174:107021. https://doi.org/10.1016/j.compositesb.2019.107021
16. Li J, Wu Z, Shi C, Yuan Q, Zhang Z. Durability of ultra-high performance concrete – a review. Construct Build Mater. 2020;255:119296. https://doi.org/10.1016/j.conbuildmat.2020.119296
17. Gao J, Sun W, Morino K. Mechanical properties of steel fiber-reinforced, high-strength, lightweight concrete. Cem Concr Compos. 1997;19(4):307–13. https://doi.org/10.1016/S0958-9465(97)00023-1
18. A. C1018. Standard test method for flexural toughness and first-crack strength of fiber-reinforced concrete (using beam with third-point loading), 1997.
19. Christidis KI, Badogiannis EG, Mintzoli C. Flexural behaviour of pumice lightweight concrete reinforced with end-hooked steel fibres. Structure. 2021;33:3835–47. https://doi.org/10.1016/j.istruc.2021.06.090
20. Hassanpour M, Shafigh P, Bin Mahmud H. Mechanical properties of structural lightweight aggregate concrete containing low volume steel fiber. Arab J Sci Eng. 2014;39(5):3579–90. https://doi.org/10.1007/s13369-014-1023-9
21. Xie J, Cong Kou S, Ma H, Long WJ, Wang Y, Ye TH. Advances on properties of fiber reinforced recycled aggregate concrete: experiments and models. Construct Build Mater. 2021;277:122345. https://doi.org/10.1016/j.conbuildmat.2021.122345
22. Zhao M, Zhao M, Chen M, Li J, Law D. An experimental study on strength and toughness of steel fiber reinforced expanded-shale lightweight concrete. Construct Build Mater. 2018;183:493–501. https://doi.org/10.1016/j.conbuildmat.2018.06.178
23. Çelik Z, Bingöl AF. Fracture properties and impact resistance of self-compacting fiber reinforced concrete (SCFRC). Mater Struct. 2020;53(3):50. https://doi.org/10.1617/s11527-020-01487-8
24. ASTM C330. Standard specification for lightweight aggregates for structural concrete. ASTM Int. 2009;552(18):4. https://doi.org/10.1520/C0330
25. ASTM C33. Concrete aggregates 1. 2010;i(C):1–11. https://doi.org/10.1520/C0033
26. Test CC, Drilled T, Concrete C. Standard test method for flexural strength of concrete (using simple beam with third-point loading) 1. *Hand.* 2010;C78-02(C):1–4. https://doi.org/10.1520/C0293
27. A. C109/109M-16a. Standard test method for compressive strength of hydraulic cement mortars (using 2-in. or cube specimens). *Annu B ASTM Stand.* 2016;i:1–10. https://doi.org/10.1520/C0109
28. ASTM C39/C39M. Standard test method for compressive strength of cylindrical concrete specimens 1. *ASTM Stand B.* 2003;i:1–5. https://doi.org/10.1520/C0039
29. ASTM C469. Standard test method for static modulus of elasticity and Poisson' s ratio of concrete in compression. *ASTM Int.* 2014;i:1–5. https://doi.org/10.1520/C0469
30. ASTM C469-11. Standard test method for splitting tensile strength of cylindrical concrete specimens. *Man Hydrocarb Anal 6th Ed.* 2008;i:545–545–3. https://doi.org/10.1520/C0469_C0469M-14
31. Chen Y, Yu QL, Brouwers HJH. Acoustic performance and microstructural analysis of bio-based lightweight concrete

containing miscanthus. Construct Build Mater. 2017;157:839–51. https://doi.org/10.1016/j.conbuildmat.2017.09.161
32. Emiroglu M, Yildiz S, Kelestemur MH. An investigation on its microstructure of the concrete containing waste vehicle tire. Comput Concr. 2008;5(5):503–8. https://doi.org/10.12989/cac.2008.5.5.503
33. ASTM C192/C192M. Standard practice for making and curing concrete test specimens in the laboratory. Am Soc Test Mater. 2016;4:1–8. https://doi.org/10.1520/C0031
34. R. I. L. E. M. TC162-TDF. Test and design methods for steel fibre reinforced concrete: bending test. Mater Struct. 2000;33:3-6.
35. ASTM C496. Standard test method for splitting tensile strength of cylindrical concrete specimens. 2008;545–545–3.
36. ASTM C1609. Standard test method for flexural performance of fiber-reinforced concrete. *ASTM Stand B.* 2012;i(C):1–8. https://doi.org/10.1520/C1609
37. Banthia N, Trottier J-F. Test methods for fexural toughness characterization of fiber reinforced concrete: some concerns and a proposition. ACI Mater J. 1995;92(1):48-57. https://doi.org/10.14359/1176
38. Smarzewski P, Barnat-Hunek D. Fracture properties of plain and steel-polypropylene-fiber-reinforced high-performance concrete. Mater Tehnol. 2015;49(4):563–71. https://doi.org/10.17222/mit.2014.180
39. Balendran RV, Zhou FP, Nadeem A, Leung AYT. Influence of steel fibres on strength and ductility of normal and lightweight high strength concrete. Build Environ. 2002;37(12):1361–7. https://doi.org/10.1016/S0360-1323(01)00109-3
40. Nodehi M, Nodehi SE. Ultra high performance concrete (UHPC): reactive powder concrete, slurry infiltrated fiber concrete and superabsorbent polymer concrete. Innov Infrastruct Solut. 2022;7(1):1-22. https://doi.org/10.1007/s41062-021-00641-7
41. Yazici Ş, Inan G, Tabak V. Effect of aspect ratio and volume fraction of steel fiber on the mechanical properties of SFRC. Construct Build Mater. 2007;21(6):1250–3. https://doi.org/10.1016/j.conbuildmat.2006.05.025
42. Chen GM, He YH, Yang H, Chen JF, Guo YC. Compressive behavior of steel fiber reinforced recycled aggregate concrete after exposure to elevated temperatures. Construct Build Mater. 2014;71:1–15. https://doi.org/10.1016/j.conbuildmat.2014.08.012
43. Shariq M, Prasad J, Masood A. Effect of GGBFS on time dependent compressive strength of concrete. Construct Build Mater. 2010;24(8):1469–78. https://doi.org/10.1016/j.conbuildmat.2010.01.007
44. Graybeal B, Davis M. Cylinder or cube: strength testing of 80 to 200 MPa (11.6 to 29 ksi) ultra-high-performance fiber-reinforced concrete. ACI Mater J. 2008;105(6):603–9. https://doi.org/10.14359/20202
45. Tokyay M, Özdemir M. Specimen shape and size effect on the compressive strength of higher strength concrete. Cem Concr Res. 1997;27(8):1281–9. https://doi.org/10.1016/S0008-8846(97)00104-X
46. Balaguru P, Foden A. Properties of fiber reinforced structural lightweight concrete. ACI Struct J. 1996;93(1). https://doi.org/10.14359/9833
47. Ye Y, Wang Z, Xie F, Fu C, Zhang Z. Mechanical properties of steel fiber reinforced high-strength lightweight aggregate concrete. Jianzhu Cailiao Xuebao/J Build Mater. 2021;24(1):63–70. https://doi.org/10.3969/j.issn.1007-9629.2021.01.009
48. Mazaheripour H, Ghanbarpour S, Mirmoradi SH, Hosseinpour I. The effect of polypropylene fibers on the properties of fresh and hardened lightweight self-compacting concrete. Construct Build Mater. 2011;25(1):351–8. https://doi.org/10.1016/j.conbuildmat.2010.06.018
49. ACI Committee 318, Building Code Requirements for Structural Concrete (ACI 318-19) and Commentary on Building Code Requirements for Structural Concrete (ACI 318R-19). 2019.
50. Iqbal S, Ali A, Holschemacher K, Bier TA. Mechanical properties of steel fiber reinforced high strength lightweight self-compacting concrete (SHLSCC). Construct Build Mater. 2015;98:325–33. https://doi.org/10.1016/j.conbuildmat.2015.08.112
51. Kayali O, Haque MN, Zhu B. Drying shrinkage of fibre-reinforced lightweight aggregate concrete containing fly ash. Cem Concr Res. 1999;29(11):1835–40. https://doi.org/10.1016/S0008-8846(99)00179-9
52. Domagała L. modification of properties of structural lightweight concrete with steel fibres/Lengvojo betono savybių modifikavimas plieninėmis fibromis. J Civil Eng Manag. 2011;17(1):36–44. https://doi.org/10.3846/13923730.2011.553923
53. Kayali O, Haque MN, Zhu B. Some characteristics of high strength fiber reinforced lightweight aggregate concrete. Cem Concr Compos. 2003;25(2):207–13. https://doi.org/10.1016/S0958-9465(02)00016-1
54. Planas J, Elices M, Guinea GV. Measurement of the fracture energy using three-point bend tests: Part 2-Influence of bulk energy dissipation. Mater Struct. 1992;25(5):305–12. https://doi.org/10.1007/BF02472671
55. Bažant ZP. Analysis of work-of-fracture method for measuring fracture energy of concrete. J Eng Mech. 1996;122(2):138–44. https://doi.org/10.1061/(ASCE)0733-9399(1996)122:2(138)
56. Hillerborg A. The theoretical basis of a method to determine the fracture energy GF of concrete. Mater Struct. 1985;18(4):291–6. https://doi.org/10.1007/BF02472919
57. Bažant ZP, Planas J. Fracture and size effect in concrete and other quasibrittle materials. London, UK: Routledge; 2019.
58. Guinea GV, Planas J, Elices M. Measurement of the fracture energy using three-point bend tests: Part 1 Influence of experimental procedures. Mater Struct. 1992;25(1992):212–8.
59. Elices M, Guinea GV, Planas J. On the measurement of concrete fracture energy using three-point bend tests. Mater Struct Constr. 1997;30(6):375–6. https://doi.org/10.1007/bf02480689
60. Bencardino F, Rizzuti L, Spadea G, Swamy RN. Experimental evaluation of fiber reinforced concrete fracture properties. Compos B Eng. 2010;41(1):17–24. https://doi.org/10.1016/j.compositesb.2009.09.002
61. Ozalp F, Akkaya Y, Sengul C, Akcay B, Tasdemir MA, Kocaturk AN. Curing effects on fracture of high-performance cement based composites with hybrid steel fibers. Proc 6th Int Conf Fract Mech Concr Concr Struct. 2007;3:1377–85.
62. Barros J, Pereira E, Ribeiro A, Cunha V, Antunes J. Self-compacting steel fibre reinforced concrete for precasted sandwich panels: experimental and numerical research. 6th Int RILEM Symp Fibre Reinf Concr – BEFIB 2004. 2004;6:11. http://repositorium.sdum.uminho.pt/handle/1822/3189
63. Hillerborg A, Modeer M, Petersson PE. Analysis of crack formation and crack growth in concrete by means of fracture mechanics and finite elements. Am Concr Inst, ACI Spec Publ. 2008;SP-249:225–37.

64. Barros JAO, Cruz JS. Fracture energy of steel fiber-reinforced concrete. Mech Adv Mater Struct. 2001;8(1):29–45. https://doi.org/10.1080/10759410119428
65. Güneyisi E, Gesoglu M, Özturan T, Ipek S. Fracture behavior and mechanical properties of concrete with artificial lightweight aggregate and steel fiber. Construct Build Mater. 2015; 84:156–68. https://doi.org/10.1016/j.conbuildmat.2015.03.054

AUTHOR BIOGRAPHIES

Jamshid Esmaeili, Department of Civil Engineering, University of Tabriz, Tabriz, Iran. Email: J-Esmaeili@tabrizu.ac.ir

Mahdi Ghaffarinia, Department of Civil Engineering, University of Tabriz, Tabriz, Iran. Email: mahdi.ghaffarinia@gmail.com

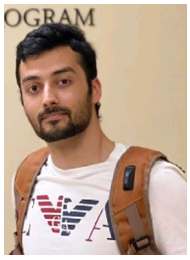

Mehrab Nodehi, Ingram School of Engineering, Texas State University, San Marcos, Texas, USA. Email: M_N224@txstate.edu

Osman Gencel, Civil Engineering Department, Faculty of Engineering, Architecture and Design, Bartin University, Bartin, Turkey. Email: ogencel@bartin.edu.tr

Jinyan Shi, School of Civil Engineering, Central South University, Changsha, China. Email: jinyan.shi@csu.edu.cn

Togay Ozbakkaloglu, Ingram School of Engineering, Texas State University, San Marcos, Texas, USA. Email: togay.oz@txstate.edu

How to cite this article: Esmaeili J, Ghaffarinia M, Nodehi M, Gencel O, Shi J, Ozbakkaloglu T. Mechanical and fractural characteristics of structural lightweight fiber reinforced concrete. Structural Concrete. 2022. https://doi.org/10.1002/suco.202200107